Redox Biology 42 (2021) 101883

Contents lists available at ScienceDirect

Redox Biology

journal homepage: www.elsevier.com/locate/redox

Research Paper

# Retinal oxidative stress activates the NRF2/ARE pathway: An early endogenous protective response to ocular hypertension

Sarah Naguib [a], Jon R. Backstrom [b], Melanie Gil [a], David J. Calkins [a,b], Tonia S. Rex [a,b,*]

[a] Department of Ophthalmology & Visual Sciences, Vanderbilt University School of Medicine, Nashville, TN, USA
[b] Vanderbilt Eye Institute, Vanderbilt University Medical Center, Nashville, TN, USA

ARTICLE INFO

*Keywords:*
Glaucoma
Nrf2
Oxidative stress
Retinal ganglion cell
Optic nerve
Antioxidant response element

ABSTRACT

Oxidative stress contributes to degeneration of retinal ganglion cells and their axons in glaucoma, a leading cause of irreversible blindness worldwide, through sensitivity to intraocular pressure (IOP). Here, we investigated early elevations in reactive oxygen species (ROS) and a role for the NRF2-KEAP1-ARE endogenous antioxidant response pathway using microbead occlusion to elevate IOP in mice. ROS levels peaked in the retina at 1- and 2-wks following IOP elevation and remained elevated out to 5-wks. Phosphorylation of NRF2 and antioxidant gene transcription and protein levels increased concomitantly at 2-wks after IOP elevation, along with phosphorylation of PI3K and AKT. Inhibiting PI3K or AKT signaling prevented NRF2 phosphorylation and reduced transcription of antioxidant-regulated genes. Ocular hypertensive mice lacking Nrf2 had elevated ROS and a diminished increase in antioxidant gene expression. They also exhibited earlier axon degeneration and loss of visual function. In conclusion, the NRF2-KEAP1-ARE pathway is endogenously activated early in ocular hypertension due to phosphorylation of NRF2 by the PI3K/AKT pathway and serves to slow the onset of axon degeneration and vision loss in glaucoma. These data suggest that exogenous activation of this pathway might further slow glaucomatous neurodegeneration.

## 1. Introduction

Glaucoma is a group of chronic optic neuropathies characterized by progressive degeneration of retinal ganglion cells (RGCs) and their axons, which transmit visual information to the brain via the optic nerve. Glaucoma is the leading cause of irreversible blindness worldwide and is characterized by age-related sensitivity to intraocular pressure (IOP) [7,29,67]. Current treatments for glaucoma aim to reduce IOP through medical or surgical intervention. Although this is relatively effective, many patients continue to experience vision loss despite these treatments [21,29,67]. Our goal is to better understand the molecular mechanisms underlying RGC degeneration and death in glaucoma in order to identify targeted therapies to protect these neurons.

RGCs and their axons are vulnerable to oxidative stress for a variety of reasons including, but not limited to, the lack of myelination along part of the axon resulting in increased metabolic demand, which is compensated for by a larger number of mitochondria [6,11,32,40,48,59]. Oxidative stress contributes to glaucoma pathogenesis in both animal models of the disease and in patients [6,26,59,70,71]. Treatment with the antioxidant α-lipoic acid reduced RGC degeneration and improved axon function in an inherited model of glaucoma (DBA2/J) [26], and treatment with valproic acid preserved RGCs in excitatory amino acid transporter 1 knockout mice (GLAST KO), which are often used as a model of normal tension glaucoma [30,31].

The retina responds endogenously to reactive oxygen species (ROS) via multiple mechanisms. For example, the retina increases expression of heat shock proteins and the anti-apoptotic Bcl-2 and Bcl-x genes in response to elevated ROS [9,24,36]. Hypoxia inducible factor-1α (HIF-1α) and Nuclear factor erythroid 2-related factor 2 (NRF2) are two transcription factors that regulate the production of antioxidant proteins [35,61]. Here we focus on the NRF2/KEAP1/ARE pathway. Under homeostatic conditions, NRF2 remains sequestered in the cytosol of the cell by Kelch-like ECH associated protein 1 (KEAP1), which targets NRF2 for ubiquitin-dependent degradation. Following increases in ROS, KEAP1 is oxidized and undergoes a conformational change resulting in the release of NRF2 and subsequent translocation into the nucleus [45,46,60,62,63]. Nuclear NRF2 interacts with small Maf proteins, and binds to the

* Corresponding author. Department of Ophthalmology & Visual Sciences, Vanderbilt University School of Medicine, Nashville, TN, USA.
*E-mail addresses:* Sarah.naguib@vanderbilt.edu (S. Naguib), Jon.backstrom@vumc.org (J.R. Backstrom), Melanie.gil@vanderbilt.edu (M. Gil), David.j.calkins@vumc.org (D.J. Calkins), Tonia.rex@vumc.org (T.S. Rex).

https://doi.org/10.1016/j.redox.2021.101883
Received 6 December 2020; Received in revised form 21 January 2021; Accepted 24 January 2021
Available online 29 January 2021

antioxidant response element (ARE) to modulate transcription of antioxidant genes. NRF2 can also undergo activation and nuclear translocation via phosphorylation by upstream signaling molecules including, but not limited to, PI3K, AKT, MAPK, JNK and GSK-3β [5,13,47,49,64].

Nrf2 knockout (KO) mice are more susceptible to RGC death following optic nerve crush and showed an increase in oxidative stress markers after injury in comparison to their wild-type controls [22,33,34]. In another study using the ischemia-reperfusion model of glaucoma, administration of an NRF2 activator was protective against RGC death. Similar findings of increased susceptibility to RGC death in Nrf2 KO mice were found in an ischemia-reperfusion model [69]. Additionally, overexpression of Nrf2 following optic nerve crush in another study increased antioxidant gene expression and protected against RGC death [20].

In this study, we report that elevation of ROS occurs early after ocular hypertension, weeks before detectable pathology or vision loss in the well-characterized microbead occlusion model of glaucoma (MOM). Further, we show that this elicits an endogenous antioxidant response mediated by NRF2 activation. Somewhat surprisingly, we show that NRF2 phosphorylation is increased; thus, the increase in ARE-driven transcripts is not due solely to oxidation of KEAP1. The increased NRF2 phosphorylation is dependent on upstream activation of PI3K or AKT. Further, the lack of Nrf2 prevents this endogenous response and results in earlier onset of axon degeneration and vision loss. Together, these data suggest that the NRF2/ARE pathway contributes to the slow onset of neurodegeneration after induction of ocular hypertension and that this pathway is a viable therapeutic target for glaucoma therapies.

## 2. Materials and METHODS

### 2.1. Mice

C57Bl/6 J (Jackson Labs, Bar Harbor, ME) or B6.129X1-*Nfe2l2*$^{tm1Ywk}$/*J* mice (Jackson Labs, Bar Harbor, ME) were group-housed, maintained on a 12-h light-dark cycle, and provided food and water ad libitum. All experiments were approved by the Institutional Animal Care and Use Committee of Vanderbilt University. Male and female mice (2–3 months old) were used for this project.

### 2.2. Microbead occlusion

We elevated IOP bilaterally using occlusion of the anterior chamber with 2 μl injections of 15-μm diameter FluoSpheres polystyrene microbeads (Thermo Fisher, Waltham, MA) as previously described [4,6,74,75]. Additional mice received bilateral injections of an equivalent volume of lactated Ringer's saline solution as controls. Briefly, 1.5 mm outer diameter/1.12 mm inner diameter filamented capillary tubes (World Precision Instruments, Sarasota, FL) were pulled using a P-97 horizontal puller (Sutter Instrument Company, Novato, CA), and the resulting needles were broken using forceps to an inner diameter of ~100 μm. Microbeads were loaded and injected using a microinjection pump (World Precision Instruments, Sarasota, FL). Mice were anesthetized with isoflurane and dilated using topical 1% tropicamide ophthalmic solution (Patterson Veterinary, Devens, MA), and 2 μl (~2000 microbeads) were injected. The needle was maintained in the injection site for 20 s before retraction to reduce microbead efflux. Mice were given topical 0.3% tobramycin ophthalmic solution (Patterson Veterinary, Devens, MA) following injection.

### 2.3. IOP measurements

We measured IOP immediately prior to microbead injection and biweekly thereafter using the Icare TonoLab rebound tonometer (Colonial Medical Supply, Franconia, NH) as previously described [6,23]. Mice were anesthetized using isoflurane, and 10 measurements were acquired from each eye within 2 min of induction of anesthesia.

### 2.4. In vivo electrophysiology

Mice were dark adapted overnight, dilated with 1% tropicamide for 10 min and anesthetized with 20/8/0.8 mg/kg ketamine/xylaxine/urethane according to previously published methodology [2,43]. Mice were placed on heated surface of the ERG system to maintain body temperature. Corneal electrodes with integrated stimulators (Celeris System, Diagnosys LLC, Lowell, MA) were placed on eyes that were lubricated with GenTeal drops. Subdermal platinum needle electrodes were placed in the snout and back of the head at the location of the visual cortex. A ground electrode was placed in the back of the mouse. For VEPs, mice were exposed to 50 flashes of 1 Hz, 0.05 cd s/m$^2$ white light with a pulse frequency of 1. For ERGs, mice were exposed to flashes of 1 Hz, 1 cd s/m$^2$ white light with a pulse frequency of 1. For photopic negative ERGs (PhNR), mice were exposed to 20 continuous flashes of white light on a green background with a pulse frequency of 2. Each experimental group had 12-16 eyes.

### 2.5. Inhibitor injections

A subset of mice (n = 20) was intravitreally injected with a PI3K inhibitor (Wortmannin, 1 μl, 10 mM, every 3 days) or vehicle (DMSO). Another subset of mice (n = 20) was injected intraperitoneally with an AKT inhibitor (Ipatasertib, 20 mg/kg every other day) or DMSO/saline one week after elevation of IOP.

### 2.6. Dihydroethidum (DHE) fluorescence

A dye that fluoresces in the presence of superoxide and, to a lesser extent, hydrogen peroxide, DHE, was utilized for these studies as previously described [2]. Mice were anesthetized with 2.5% isofluorane and intravitreally injected with 1 μl (0.5 μM) of DHE (ThermoFisher Scientific, Waltham, MA) diluted in phosphate-buffered saline (PBS) using a 30-gauge Hamilton syringe. Just prior to imaging, mice were anesthetized with ketamine/xylazine and eyes were dilated with 1% tropicamide. Thirty minutes after DHE injection, fluorescence was imaged on a Micron IV retinal imaging microscope (Phoenix Research Labs, Pleasanton, CA) using an FF02-475/50 nm excitation filter (Semrock, Inc. Rochester, NY) and ET620/60X emission filter (Chroma Technology Corp., Bellows Falls, VT). The average intensity of the fluorescence throughout the retina was quantified using ImageJ (Rasband, W.S., 2018). For each experimental group, 6–8 eyes were analyzed. For purposes of comparison, the 2-wk wildtype data from Fig. 2 is reshown in Fig. 6 to compare to Nrf2 KO mice.

### 2.7. Tissue collection

For western blots and qPCR, retinas were collected and flash frozen from mice euthanized by anesthetic overdose and cervical dislocation. For immunohistochemistry and optic nerve histology, tissue was collected and incubated in 4% paraformaldehyde until use at 4 °C.

### 2.8. Protein assay

Protein concentrations were determined from 10 μl of retina homogenates with the Pierce BCA Protein Assay Kit (cat#: 23225, ThermoFisher Scientific, Waltham, MA). BSA was used as the protein standard. Absorbance was measured with the plate reader POLARstar Omega (BMG Labtech, Ortenburg, Germany).

### 2.9. Western blot

Single retinas were sonicated in lysis buffer (PBS, EDTA and Halt protease inhibitor) and centrifuged for 30 min at 4 °C. 4x Laemmli buffer

(Bio-rad, cat# 1610747) containing 2-β-mercaptoethanol was added to the samples and heated for 5 min at 95 °C. Known amounts of protein (10–20 μg/retina) or protein ladder (cat#1610375, Bio-rad, Hercules, CA) were loaded in 4–20% polyacrylamide gels (Bio-Rad #456–1095). Proteins were transferred onto nitrocellulose using the Bio-Rad trans blot turbo transfer system. Membranes were blocked in 2% BSA in TBS overnight at 4 °C. Membranes were incubated in primary antibody (see Table 1) at room temperature with rocking for 2 h $\beta$-actin was used as the loading control for all experimental groups. After washing, membranes were incubated with secondary antibody (IRDye 800CW Donkey anti-rabbit, #926–32213 or IRDye 680CW Donkey anti-mouse, #926–68022,1:5000 in 1% BSA/TBS) at room temperature for 1 h. After washing, blots were imaged with a Bio-Rad ChemiDoc system. Band density was quantified by scanning the blot using Adobe Photoshop. Each band was selected with the same frame and set measurements were used to obtain the gray mean value for each. Band intensity measurements from protein of interest were divided by band intensity measurements of loading control (β-actin). Each experimental group had 5 retinas. For purposes of comparison, the 2-wk wild-type data in Fig. 3 was reshown in Fig. 6 to compare to Nrf2 KO data.

### 2.10. Co-immunoprecipitations

Single retinas were sonicated in 300 μl lysis buffer (1% SDS, 5 mM EDTA and Halt protease inhibitor) and centrifuged for 30 min at 4 °C. Supernatant was collected and placed on ice. Lysates were pre-cleared using normal serum for 1 h on ice. 1–5 μl of antibody (see Table 1) was added after supernatant was separated in a clean microcentrifuge tube and incubated overnight at 4 °C rocking. 70 μl Protein G-coupled Sepharose beads were added on ice to each sample and incubated at 4 °C under agitation for 4 h. Beads were washed with lysis buffer 3 times to remove nonspecific binding. Then 50 μl of beads were eluted by using 50 μl of 2x SDS with DTT. Samples were boiled at 95 °C for 5 min and analyzed via Western blot as stated above.

### 2.11. Quantitative PCR

Retinas were extracted from euthanized mice and placed immediately onto dry ice and stored at $^{-}80^{o}$C until homogenized by hand using 1.5 ml-capacity pestles (cat#46C911, Grainger, Nashville, TN). RNA was extracted using a Qiagen RNeasy kit (Valencia, CA) as previously described [23]. RNA concentration and purity were measured on a spectrophotometer. First-strand complementary DNA (cDNA) was synthesized from 250 ng of RNA from each sample using the Superscript III First-Strand synthesis system and oligo-dT20 primers (Invitrogen, Waltham, MA). Quantitative PCR (qPCR) was performed using Power SYBR green master mix (Applied Biosystems, Waltham, MA). All primer sequences were obtained from previous studies; we assessed the following: *Nrf2*, *Prdx6*, *Gpx1*, *Txn1*, *Hif1α*, *Sod2* and *Sod3* (see Table 2). All qPCR was performed in duplicate using an Applied Biosciences 7300 real-time PCR system (Waltham, MA). The assay was performed in triplicate on 5 retinas per condition. The amplification threshold was set using system software. Relative changes in gene expression were determined using GAPDH as the internal control. Each experimental group had 5 retinas.

**Table 1**
Western blot antibodies.

| Protein | Catalog number | Company | Dilution | Species |
|---|---|---|---|---|
| NRF2 | 137550 | Abcam | 1:600 | Rabbit |
| Phosphorylated NRF2 (Ser40 residue) | PA5-67520 | ThermoFisher | 1:1000 | Rabbit |
| Superoxide Dismutase 2 (SOD2) | 13533 | Abcam | 1:1000 | Rabbit |
| ß actin | 4967S | Cell Signaling | 1:1000 | Rabbit/ mouse |
| PI3K | 4257 | Cell Signaling | 1:1000 | Rabbit |
| Phosphorylated PI3K | 4228 | Cell Signaling | 1:1000 | Rabbit |
| AKT | 4685 | Cell Signaling | 1:500 | Rabbit |
| Phosphorylated AKT | 4060 | Cell Signaling | 1:500 | Rabbit |
| SAPK/JNK | 9252 | Cell Signaling | 1:1000 | Rabbit |
| Phosphorylated JNK | 4668 | Cell Signaling | 1:1000 | Rabbit |
| GSK3β | 12456 | Cell Signaling | 1:500 | Rabbit |
| Phosphorylated GSK3β | 5558 | Cell Signaling | 1:2000 | Rabbit |
| MAPK/ERK1/2 | 4695 | Cell Signaling | 1:1000 | Rabbit |
| Phosphorylated MAPK/ ERK1/2 | 4370 | Cell Signaling | 1:1000 | Rabbit |
| Superoxide dismutase 3 (SOD3) | 80946 | Abcam | 1:1000 | Mouse |
| Glutathione peroxidase 1 (GPX1) | PA5-26323 | ThermoFisher | 1:1000 | Rabbit |
| Peroxiredoxin 6 (Prdx6) | 59543 | Abcam | 1:500 | Rabbit |
| HIF-1α | 36169S | Cell Signaling | 1:1000 | Rabbit |
| NQO-1 | 62262S | Cell Signaling | 1:1000 | Rabbit |
| HO-1 | 82206S | Cell Signaling | 1:1000 | Rabbit |

### 2.12. PCR microarray

The same cDNA used for the quantitative PCR analysis was also used in an RT2 Profiler mouse oxidative stress PCR array kit per manufacturer's instructions (Qiagen, Valencia, CA) as previously described [23]. The cDNA from each group was pooled to have sufficient material for the assay. Each experimental group had 5 pooled retinas.

### 2.13. Immunohistochemistry

Eyes stored in paraformaldehyde were embedded in Tissue Freezing Medium (Electron Microscopy Sciences) overnight, and 10-μm-thick sections were collected on a cryostat. Cross sections were incubated overnight at 4 °C in PBS containing 5% normal donkey serum (Millipore Sigma, #D9663, St. Louis, MO), 0.1% Triton X-100, 0.5% BSA, and 0.1% sodium azide (PBTA). Retina sections were then incubated overnight at 4 °C with rabbit anti-nitrotyrosine (Millipore Sigma, Burlington, MA #AB5411; 1:400) with or without mouse anti-NeuN (Millipore Sigma # MAB377X, 1:400) in PBTA, rinsed with PBTA, and then incubated overnight at 4 °C with Alexa Fluorophore donkey secondary antibodies (ThermoFisher anti-rabbit 488 #R37118; 1:200, and anti-mouse 555 #R37118; 1:200 in PBTA. After extensive washing, sections were mounted with DAPI (ThermoFisher Scientific, Waltham, MA). Slides were imaged on a Nikon Eclipse epifluorescence microscope (Nikon, Melville, NY). All images were collected from the same retinal region with identical magnification, gain and exposure settings. Fluorescence intensity was quantified via ImageJ as previously described [43,53]. A rectangle was selected around the region of interest, channels were split for multiple antibodies, threshold was adjusted, noise was de-speckled and fluorescence intensity was measured. Fluorescence intensity was normalized to saline-injected mice. Each experimental group included 5 eyes.

### 2.14. Optic nerve counts

Optic nerves were post-fixed in glutaraldehyde followed by Resin 812 embedding and Araldite 502 (cat#: 14900 and 10900 respectively,

**Table 2**
qPCR primers.

| Gene | Forward Primer | Reverse Primer |
|---|---|---|
| Nrf2 | CCA GCT ACT CCC AGG TTG C | CCA AAC TTG CTC CAT GTC CT |
| Prdx6 | TTG ATG ATA AGG GCA GGG AC | CTA CCA TCA CGC TCT CTC CC |
| Gpx1 | GGTTCGAGCCCAATTTTACA | CCCACCAGGAACTTCTCAAA |
| Txn1 | ATG ACT GCC AGG ATG TTG C | CCT TGT TAG CAC CGG AGA AC |
| HIF1α | CCT GCA CTG AAT CAA GAG GTG C | CCA TCA GAA GGA CTT GCT GGC T |
| SOD2 | GAC AAA CCT CAG CCC TAA CG | GAA ACC AAG CCA ACC CCA AC |
| SOD3 | AGGTGGATGCTGCCGAGAT | TCCAGACTGAAATAGGCCTCAAG |

Electron Microscopy Sciences, Hatfield, PA) according to previously published protocols [2,23,43]. Leica EM-UC7 microtome was used to collect 1 μm thick sections of the optic nerves. Sections were then stained with 1% paraphenylenediamine and 1% toluidine blue and were imaged on a Nikon Eclipse Ni-E microscope using 100× oil immersion objective (Nikon Instruments, Melville, NY). The optic nerves were montaged into a 5 × 5 image using the Nikon Elements software to scan a large image. The Counting Array and Better Cell Counter plugins to ImageJ, which creates a grid of nine squares overtop the montaged optic nerve, were used. Healthy and degenerating axons, which are color-coded by the plugins, were manually counted. Degenerative axon profiles were identified by dark paraphenylenediamine staining due to collapsed myelin or loose myelin (onioning) surrounding the axon. A grid was used to avoid bias, by always counting in the same squares, using a cross configuration. Twenty percent of the optic nerve cross-sectional area was counted and the total was multiplied by five to estimate total and degenerating axons within the nerve. Each experimental group included 4–5 nerves.

## 3. Data analysis

All statistical analyses were performed using GraphPad Prism software (La Jolla, CA). A one-way ANOVA with a Bonferroni post hoc test ($\alpha = 0.05$) was used to analyze Western blot quantification, IHC fluorescence quantification, ON quantification data, and ERG/VEP latencies and amplitudes. A one-way ANOVA and Dunnett's multiple comparisons

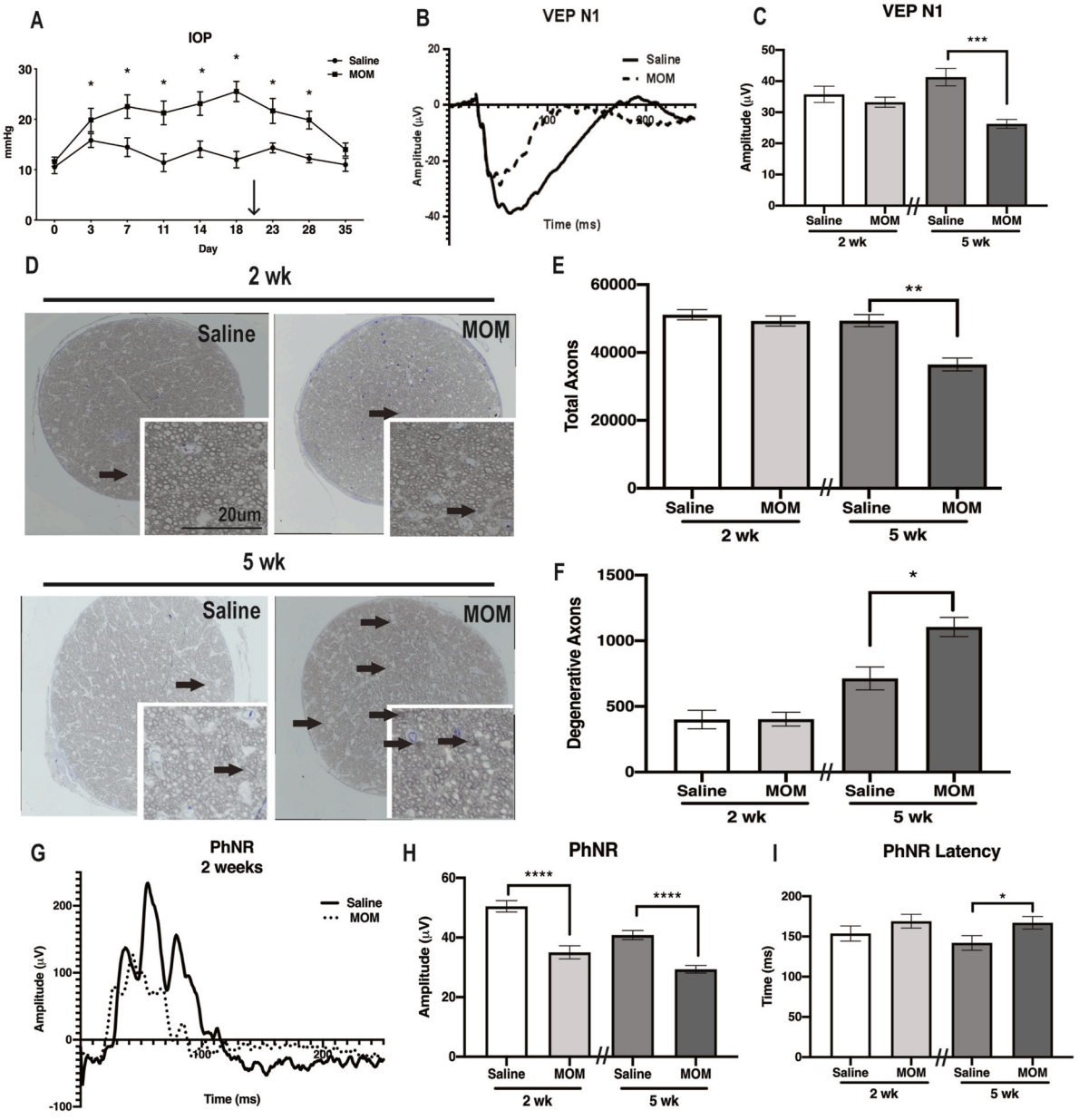


**Fig. 1.** Visual function and optic nerve structure at 2- and 5-weeks post-IOP elevation. A) IOP levels over time, arrow indicates re-injection of microbeads, *p < 0.05. B) Representative VEP N1 waveforms, showing decreased amplitude in 5wk MOM-injected mice. C) Quantification of VEP N1 amplitude, ***p < 0.001. D) Representative micrographs of optic nerves, insets show higher magnification. Scale bar applies to all insets. Arrows indicate degenerative axons. E) Quantification of total axons in the optic nerves, showing a decrease only at 5 wk post-IOP elevation, p < 0.01. F) Quantification of number of degenerative axons, showing an increase at 5 wks, *p < 0.05. G) Representative waveforms of photopic negative response (PhNR) amplitude in saline and 2-week post-IOP elevation mice. H) and I) Quantification of the PhNR amplitude and latency, showing decreases in amplitudes at both timepoints and an increase in latency at 5-wks, *p < 0.05, ****p < 0.0001.

post hoc test ($\alpha = 0.05$) were used to analyze the qPCR results. Means and standard deviation were calculated for each data set.

## 4. Results

### 4.1. Reduction in PhNR precedes axon degeneration and VEP deficits

After injection of microbeads, IOP remained elevated for the duration of the study (Fig. 1A). When IOP began decreasing in a subset of mice, we reinjected microbeads (arrow in Fig. 1A). IOP elevation caused a reduction in the VEP amplitude 5-wks later ($p < 0.0001$, Fig. 1B and C) in agreement with previous studies from our lab [4,23]. In comparison, the VEP amplitude was unaffected at 2-wks post-IOP elevation (Fig. 1C). The total number of axons was decreased and the number of degenerative axons was increased in the 5-wk post-IOP elevation group in comparison to saline-injected controls ($p = 0.0011$, Fig. 1D–F), similar to our previous studies [4,8,23]. In contrast, at 2-wks post-IOP elevation, there was no evidence of axon degeneration or axon loss in the ocular hypertensive optic nerves as compared to saline controls (Fig. 1D–F).

The VEP is recorded from the visual cortex and thus does not directly measure activity from the optic nerve. A direct measure of RGC physiological function might be more sensitive to glaucomatous changes. This is supported by recently demonstrated changes in single cell RGC physiology at 2-wks post-IOP elevation [55]. Therefore, we measured

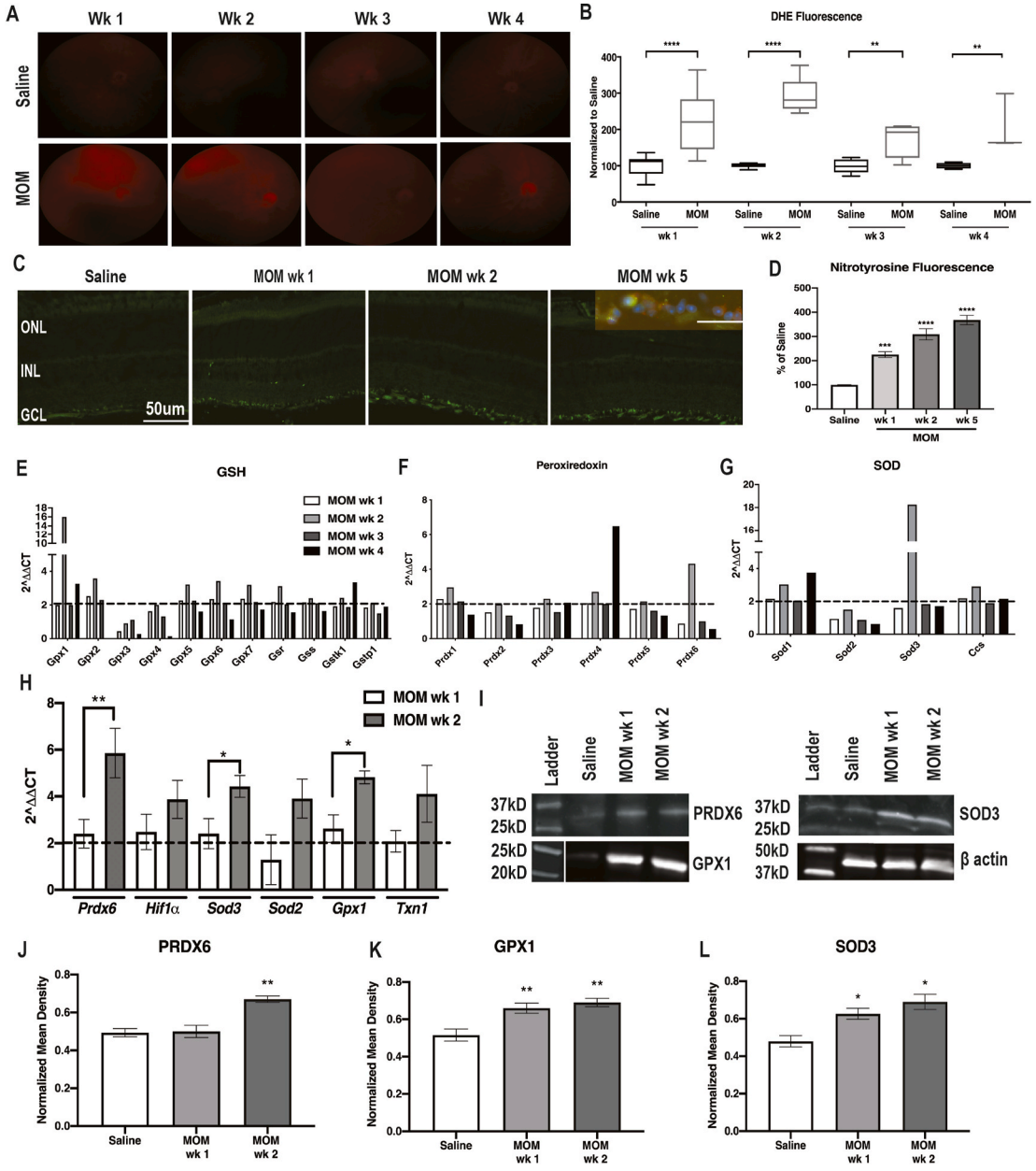


**Fig. 2.** ROS and antioxidant proteins increased at 1-wk and 2-wks post-IOP elevation. A) Representative fundus images of DHE fluorescence in all groups. B) Quantification of DHE fluorescence at 1–4 wks post-IOP elevation in comparison to saline-injected controls, showing increases in the microbead injected mice at all time points, $^{**}p < 0.001$, $^{****}p < 0.0001$. C) Fluorescence micrographs of retinas labeled with DAPI (blue) and nitrotyrosine (green). Inset shows double-labeling with anti-nitrotyrosine (green) and anti-NeuN (red). D) Quantification of nitrotyrosine immunofluorescence showing increases at all timepoints after IOP elevation, $^{***}p < 0.001$, $^{****}p < 0.0001$. E-G) Quantification of fold changes in PCR microarray for: E) GSH-related genes; F) Peroxiredoxin-related genes; and G) SOD-related genes. Dotted line indicates threshold for increase compared to saline. H) Confirmatory qPCR for fold change over saline in antioxidant gene transcription, $^{*}p < 0.05$, $^{**}p < 0.01$. I) Representative western blots for β-actin, PRDX6, SOD3 and GPX1. J-L) Quantification of PRDX6, SOD3 and GPX1, respectively, after normalization to β-actin, $^{*}p < 0.05$, $^{**}p < 0.001$. (For interpretation of the references to color in this figure legend, the reader is referred to the Web version of this article.)

the photopic negative response (PhNR), which is a part of the cone ERG pathway. We detected a significant decrease in the PhNR amplitude at both 2-wks (n = 12) and 5-wks (n = 14) post-IOP elevation in comparison to saline-injected controls, p = 0.0019 and p < 0.001, respectively (Fig. 1G and H). PhNR latency was unaffected at 2-wks post-IOP elevation, but was increased at 5-wks (p = 0.0441, Fig. 1I).

### 4.2. Increased ROS and an endogenous retinal antioxidant response occur early in ocular hypertension

The level of retinal superoxide was increased at 1-wk (n = 12) and 2-wks (n = 8) post-IOP elevation in comparison to saline-injected controls, based on DHE fluorescence, p < 0.0001 for both (Fig. 2A and B). DHE fluorescence was elevated to a lesser extent at 3- and 4-wks post-IOP elevation (n = 6 eyes/group, p = 0.0086 and p = 0.0048, respectively) (Fig. 2A and B). As a further assessment of oxidative stress, we immunolabeled with nitrotyrosine (Fig. 2C). Nitrotyrosine immunofluorescence was detected specifically within the ganglion cell layer (GCL) at all timepoints post-IOP elevation (Fig. 2C). To determine if the anti-nitrotyrosine labeled astrocytes or neurons, we co-labeled with NeuN (Fig. 2C, inset). Co-labeling was present indicating that nitrotyrosine was increased in the neurons of the GCL (Fig. 2C inset). Unfortunately, the nitrotyrosine antibody was produced in the same species as the RGC-specific antibody, RPBMS, so we were unable to determine if the labeling is specific to RGCs or is also present in displaced amacrine cells. Quantification of the anti-nitrotyrosine fluorescence showed a statistically significant increase in all MOM groups compared to saline controls (n = 5 eyes/group, p < 0.0001, F = 51.6, Fig. 2D). Nitrotyrosine fluorescence increased significantly between 1- and 5-wks post-IOP elevation (p = 0.0015, Fig. 2D) but not between 2- and 5-wks.

Next, we wanted to determine if the retina endogenously responds to the increases in ROS. Using an oxidative stress PCR array, we detected increased expression of the antioxidant enzymes *Prdx6, Gpx1, Gpx2, Gpx5, Gpx6, Gpx7, Gsr, Sod1* and *Sod3* that was greatest at 2-weeks post-IOP elevation (Fig. 2E–G). Using qPCR, we confirmed a statistically significant increase in expression for *Prdx6* (p = 0.0094), *Sod3* (p = 0.0436) and *Gpx1* (p = 0.0148) as compared to saline-injected controls (Fig. 2H). In order to determine if there was also an increase at the protein level, we performed Western blot analysis for these three representative antioxidant enzymes. PRDX6 was increased at 2-wks post-IOP elevation (n = 5 retinas/group, p = 0.0002, F = 23.72) (Fig. 2I and J). Both GPX1 and SOD3 were increased at both 1- and 2-wks post-IOP elevation in comparison to saline-injected controls (n = 5 retinas/group, p = 0.0014, F = 14.44 and p = 0.0013, F = 11.78, respectively) (Fig. 2I, K, L).

### 4.3. NRF2 is released from KEAP1 and activated via phosphorylation

Since one of the major pathways that controls expression of these genes is the NRF2-KEAP1-ARE pathway, we next investigated activation of this pathway in ocular hypertension. *Nrf2* mRNA levels trended down at 2-wks post-IOP elevation, but did not reach statistical significance (n = 5 retinas/group, p = 0.33; Fig. 3A). There was also no difference in NRF2 protein levels at any timepoint assessed as compared to saline-injected controls, (n = 5 retinas/group, p = 0.97, F = 0.0769) (Fig. 3B and C). NRF2 can become activated either by oxidation of its repressor protein, KEAP1, which targets the protein for degradation via ubiquitination [25,46,47,63], or by phosphorylation of NRF2 (pNRF2). We

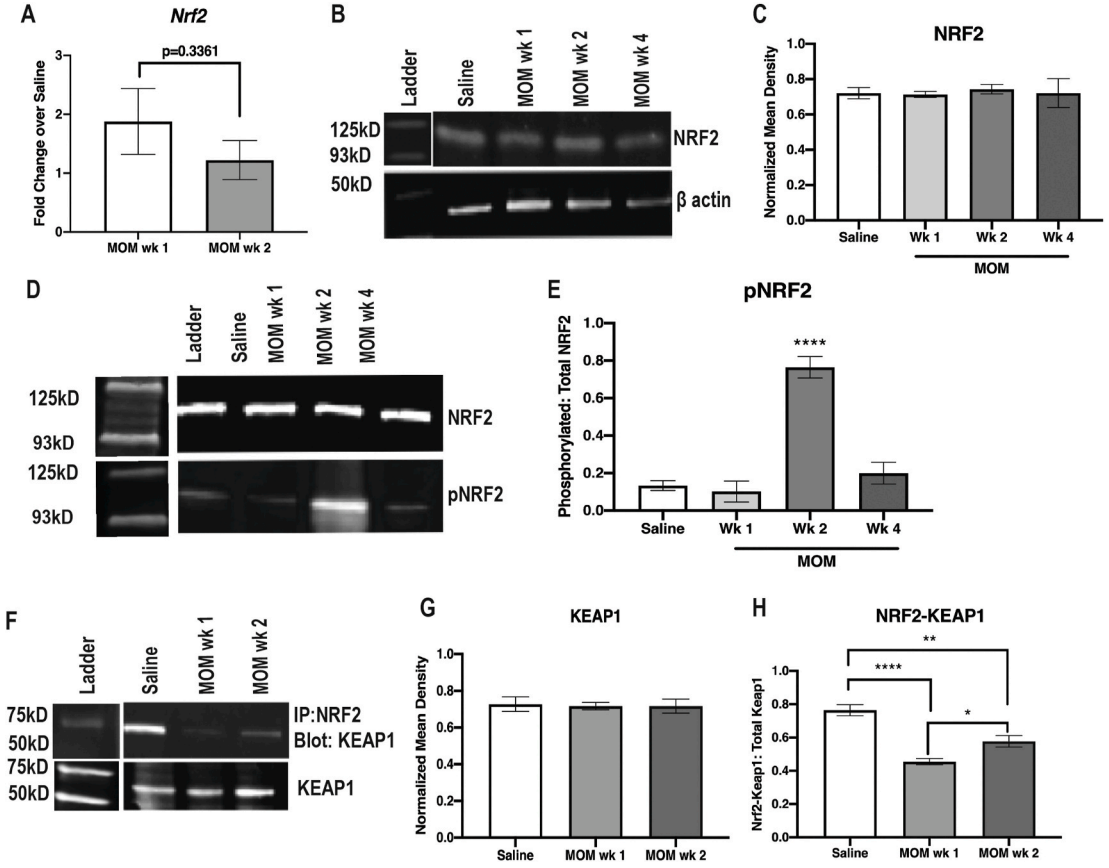


**Fig. 3.** Nrf2 activation following ocular hypertension. A) Quantification of *Nrf2* mRNA. B) Representative western blots of NRF2. C) Quantification of NRF2 Western blot after normalization to β-actin. D) Representative western blots for total and phosphorylated NRF2. E) Quantification of pNRF2 after normalization to total NRF2, ****p < 0.00001. F) Representative KEAP-1 western blots with or without immunoprecipitation of NRF2. G, H) Quantification of total KEAP-1. I) Quantification of KEAP-1 that immunoprecipitated with NRF2, *p < 0.05, **p < 0.001, ****p < 0.00001.

detected a significant, transient, increase in NRF2 phosphorylation at 2-wks post-IOP elevation in comparison to all other groups (n = 5 retinas/group, p < 0.0001, F = 23.36, Fig. 3D and E). We used co-immunoprecipitation to assess the amount of NRF2 bound to its repressor protein, KEAP1. There was no difference in total KEAP1 protein levels in saline-injected controls or at any timepoint post-IOP elevation (n = 5 retinas/group, p = 0.9701, F = 0.0305) (Fig. 3F and G). In addition, the association between NRF2 and KEAP1 was decreased in the ocular hypertensive mice as compared to saline controls (p = 5 retinas/co-IP; p < 0.0001, F = 26.72; Fig. 3F, H). There was a slight, but statistically significant increase in association between KEAP1 and NRF2 at 2-wks than at 1-wk (p = 0.0155, Fig. 3F, H).

### 4.4. NRF2 is activated by AKT/PI3K signaling

Several upstream signaling molecules can phosphorylate NRF2, including but not limited to, PI3K, AKT, JNK, GSK3β and ERK [5,47,64,76]. There were no differences in total to phosphorylated GSK3β, JNK, or ERK at 1- or 2-wks post-IOP elevation as compared to saline controls (data not shown). In contrast, phosphorylated AKT (pAKT) was significantly increased at 1- and 2-wks post-IOP elevation in comparison to saline injected controls (n = 5 retinas/group, p = 0.0185, F = 6.416) (Fig. 4A and B). In order to determine if NRF2 activation was dependent on phosphorylation by AKT, we treated ocular hypertensive mice with the AKT inhibitor, Ipatasertib, intraperitoneally at 7, and 10 days post-IOP elevation and collected retinas at 2-wks post-IOP elevation (n = 10 mice/group) (Fig. 4C). Ipatasertib targets the ATP-binding domain that targets active pAKT [56]. Inhibition of pAKT prevented the increase in gene expression of *Gpx1* and *Txn1* (p = 0.0019 and p = 0.0042 respectively, Fig. 4D). Additionally, Ipatasertib treatment reduced phosphorylation of NRF2 (p = 0.0009, Fig. 4E and F). Further, Ipatasertib treatment prevented increases in PRDX6 (p = 0.0015), GPX1 (p = 0.0001) and SOD3 (p = 0.0002) levels in the ocular hypertensive mice (Fig. 4G–J).

Phosphorylation of PI3K (pPI3K) was also significantly increased at 1- and 2-wks post-IOP elevation in comparison to saline-injected controls (p < 0.0001, F = 130.5; Fig. 5A and B). In order to determine if NRF2 activation following ocular hypertension is dependent on phosphorylation by PI3K, we treated with the PI3K inhibitor, Wortmannin, intravitreally at 7 and 10-days post-IOP elevation and then collected at

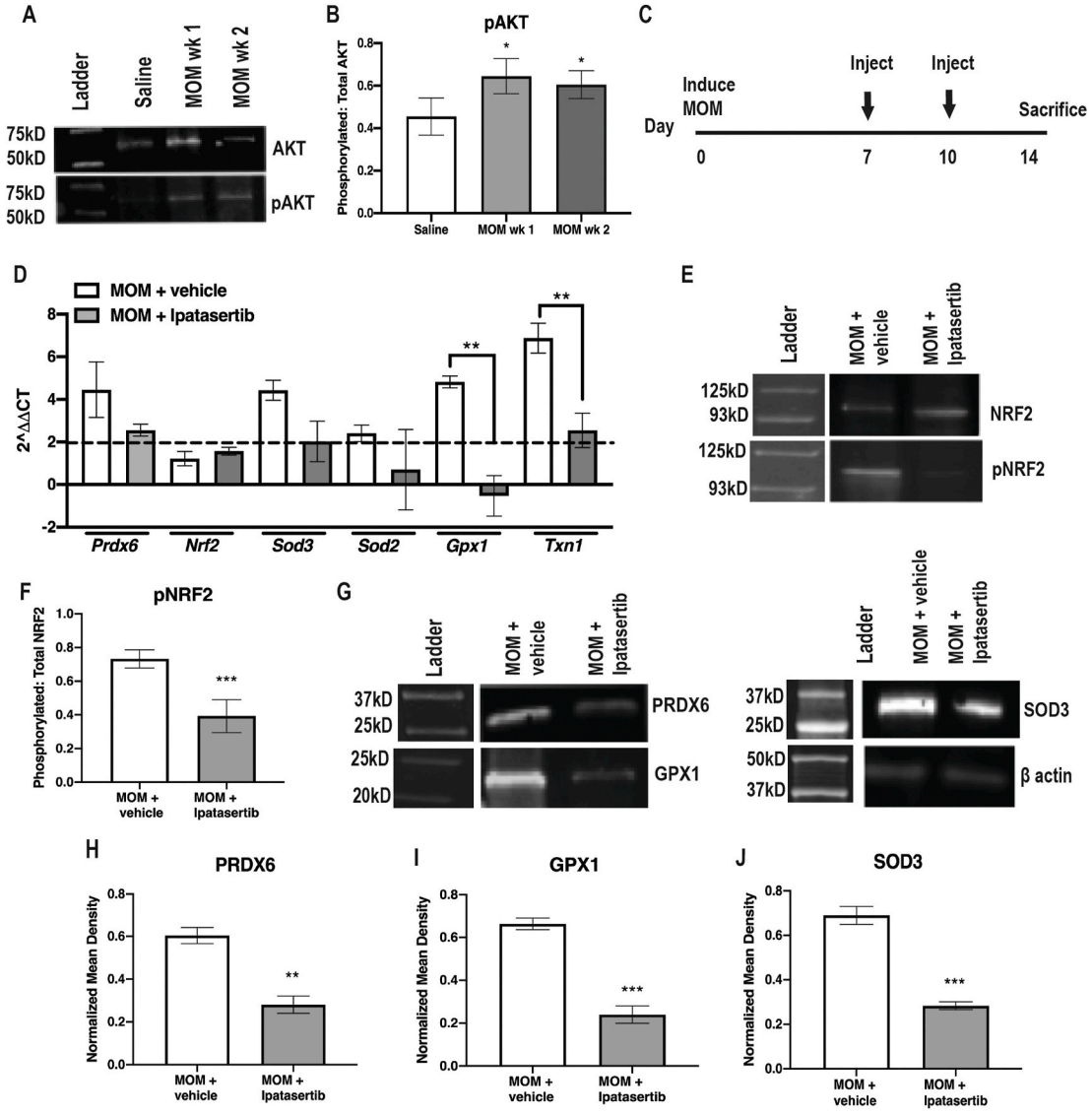


**Fig. 4.** AKT-dependent NRF2 phosphorylation. A) Representative western blots of AKT and pAKT B) Quantification of pAKT to total AKT, *p < 0.05. C) Experiment timeline. D) Representative Western blot of phosphorylated NRF2 to total NRF2. E) Quantification of pNRF2 to total NRF2, ***p < 0.0001. F) Quantification of antioxidant gene transcription shown as fold change over saline, **p < 0.001. G) Representative western blots for β-actin, PRDX6, SOD3 and GPX1. H-J) Quantification of PRDX6, GPX1 and SOD3, respectively, after normalization to β-actin, **p < 0.001, ***p < 0.0001.

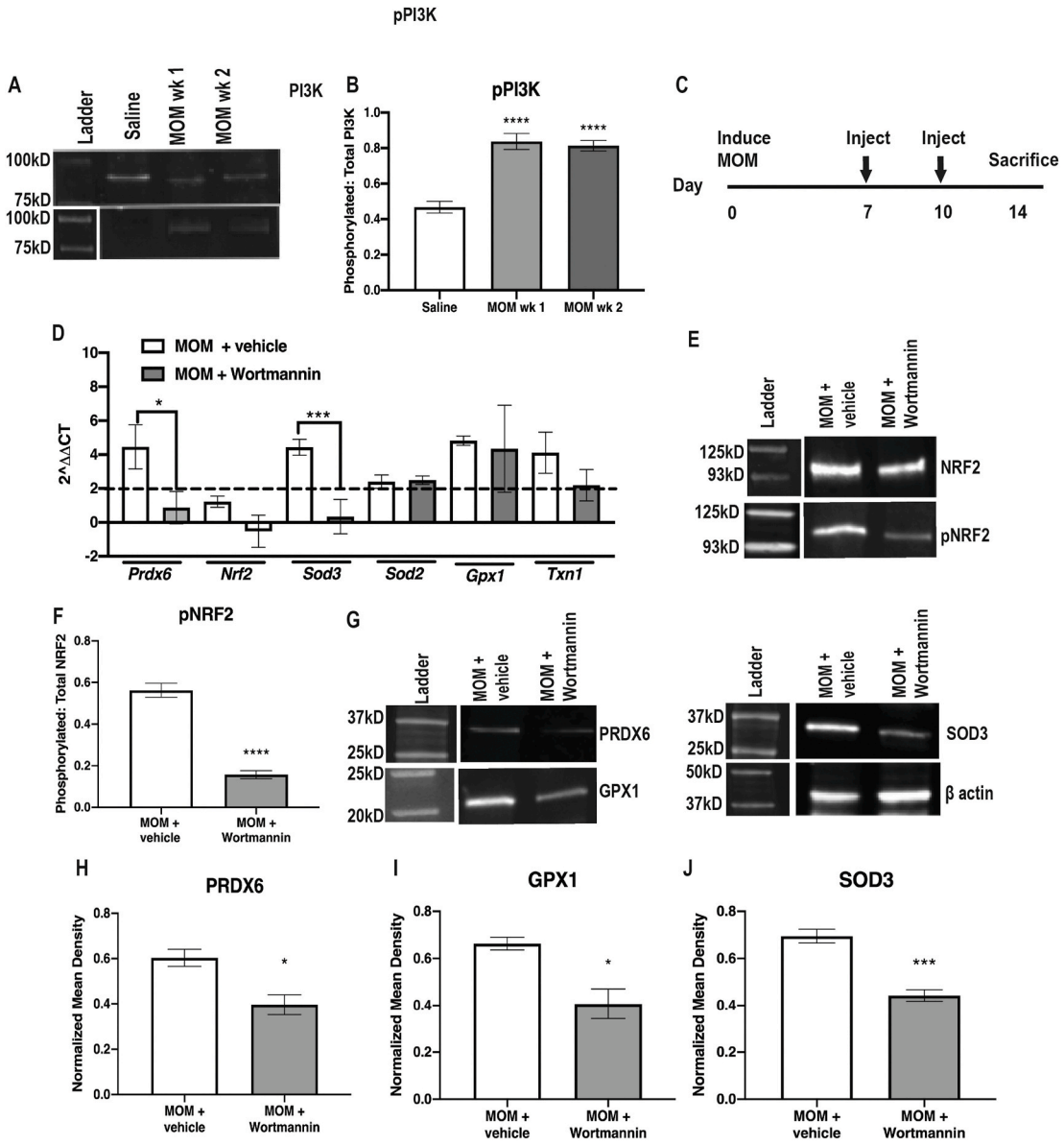


**Fig. 5.** PI3K-dependent NRF2 phosphorylation. A) Representative western blots of PI3K and pPI3K B) Quantification of pPI3K to total PI3K, ****p < 0.00001. C) Experiment timeline. D) Representative western blots of pNRF2 to total NRF2. E) Quantification of pNRF2 to total NRF2, ****p < 0.00001. F) Quantification of antioxidant gene transcription shown as fold change over saline, *p < 0.05, ***p < 0.0001. G) Representative western blots for β-actin, PRDX6, SOD3 and GPX1. H-J) Quantification of PRDX6, GPX1 and SOD3, respectively, after normalization to β-actin, *p < 0.05, ***p < 0.0001.

2-wks (Fig. 5C). Wortmannin inactivates PI3K activity by forming a covalent adduct with Lys802 of PIK3CD [68]. The inhibitor prevented the increase in expression of *Prdx6* and *Sod3*, p = 0.0397 and p = 0.0105, respectively (Fig. 5D). NRF2 phosphorylation was also reduced in the inhibitor-treated animals as compared to vehicle controls (p < 0.0001, Fig. 5E and F). Further, there was a lack of increase in levels of PRDX6 (p = 0.0231), GPX1 (p = 0.0209) and SOD3 (p = 0.0006) in Wortmannin injected animals (Fig. 5G–J).

### 4.5. Ocular hypertensive Nrf2 KO mice have earlier onset axon degeneration

Since antioxidant protein expression can be induced through other, non-NRF2 mediated pathways, we used Nrf2 KO mice to assess the importance of this pathway on the endogenous antioxidant response of the retina. Nrf2 KO mice are highly susceptible to oxidative stress and accelerated neurodegeneration [8,16,44]. In comparison to the wild-type counterparts, there was a significant increase in DHE fluorescence in the saline-injected Nrf2 KO mice, p = 0.0001 (Fig. 6A and B). Interestingly, there was no difference in the level of DHE fluorescence between the saline and microbead injected Nrf2 KO mice, p = 0.1867 (Fig. 6A and B). Out of the six antioxidant proteins we assessed, gene expression was not elevated in four of them. Further, the levels of gene expression in the Nrf2 KO retinas were statistically significantly lower than in the wild-type retinas for: *Prdx6* (p = 0.0067), *Sod3* (p = 0.054), *Sod2* (p = 0.0220), *Gpx1* (p = 0.0003) (Fig. 6C). The expression levels of Hif1α and Sod3 were still elevated compared to the Nrf2 KO saline group. Similarly, protein levels of PRDX6, GPX1, and SOD3 were not increased in Nrf2 KO ocular hypertensive mice as compared to their saline controls, unlike in wild-type mice at 2-wks post-IOP elevation (Fig. 6D–G). In fact, basal levels of these proteins were also reduced in the Nrf2 KO saline-injected controls compared to the saline-injected wild-type controls (p = 0.0349, p = 0.0312, and p = 0.054 for PRDX6, GPX1, and SOD3, respectively; Fig. 6E–G).

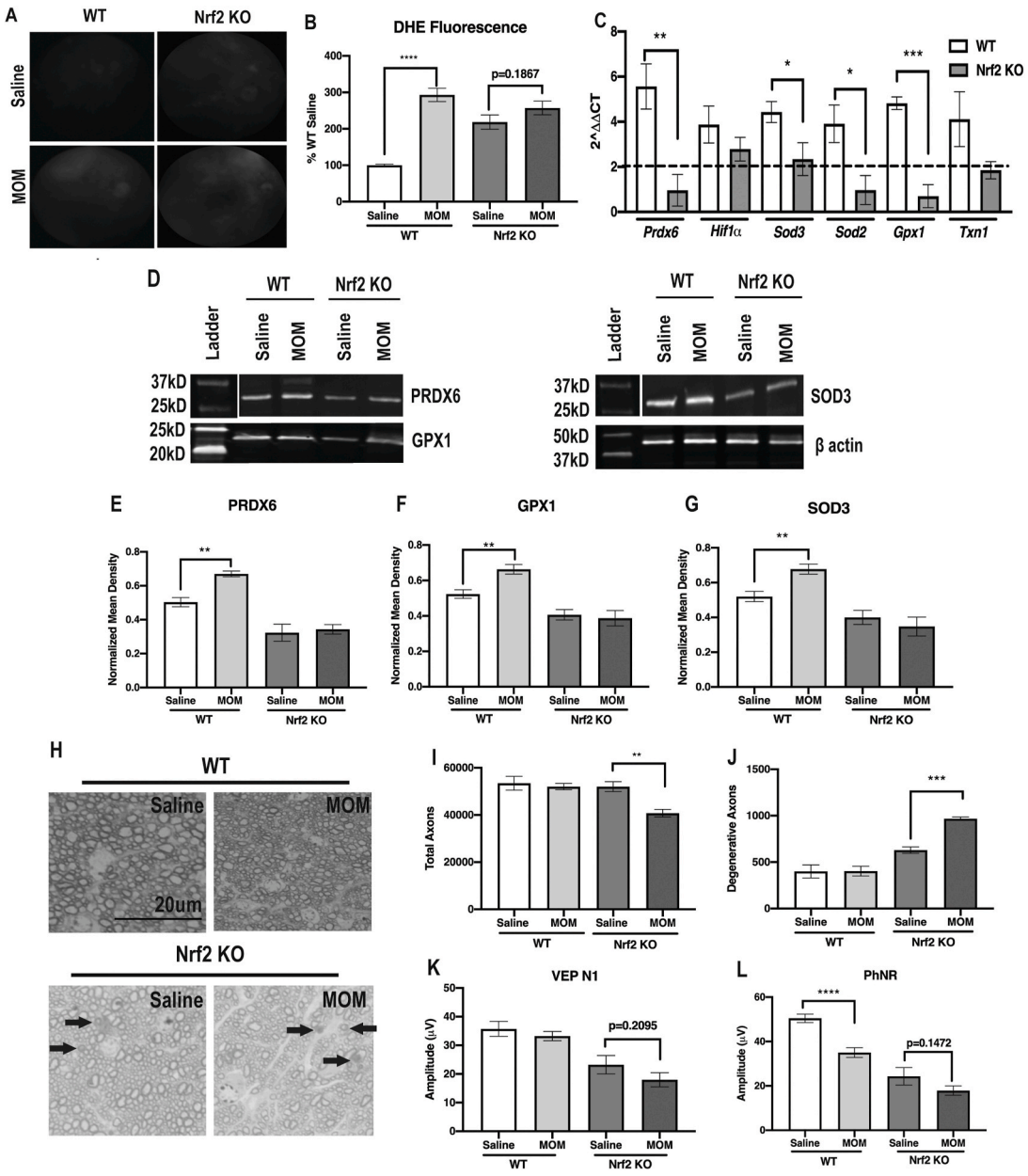


**Fig. 6.** Decreased antioxidants and increased ROS, axon degeneration, and visual function deficits in ocular hypertensive Nrf2 KO mice. A) Representative fundus images of DHE fluorescence in saline and microbead-injected wildtype and Nrf2 KO mice. B) Quantification of DHE fluorescence at 2-wks post-IOP elevation in both strains of mice. C) Quantification of antioxidant gene transcription shown as fold change over respective saline groups, *$p < 0.05$, **$p < 0.001$, ***$p < 0.0001$. D) Representative western blots for β-actin, PRDX6, SOD3 and GPX1. E-G) Quantification of PRDX6, GPX1 and SOD3, respectively, after normalization to β-actin, **$p < 0.001$. H) Representative micrographs of wildtype and Nrf2 KO optic nerves at 2-wks post-IOP elevation. Scale bar applies to all micrographs. Arrows indicate degenerative axons. I) Quantification of total axons in the optic nerves, showing a decrease only in ocular hypertensive Nrf2 KO mice, **$p < 0.001$. J) Quantification of number of degenerative axons, showing an increase in ocular hypertensive Nrf2 KO mice, ***$p < 0.0001$. K) Quantification of the N1 amplitude of the VEP. L) Quantification of the PhNR amplitude. Note: all wild-type data shown in this Figure was copied from Fig. 2 for purposes of comparison.

Next, we assessed if this lack of endogenous antioxidant response increased the susceptibility of the RGC axons to degeneration following IOP elevation. Degenerative axons were present in the optic nerves of both the saline and microbead injected Nrf2 KO mice unlike in the wild-type mice (Fig. 6H). Quantification of the number of total optic nerve axons showed fewer axons in the microbead-injected Nrf2 KO mice in comparison to Nrf2 KO saline-injected controls, $p = 0.0054$ (Fig. 6I). There was no difference between the wild-type or Nrf2 KO saline-injected controls, $p = 0.6966$ (Fig. 6I). More degenerative axons were detected in the optic nerves of Nrf2 KO ocular hypertensive mice in comparison to the Nrf2 KO saline-injected controls, $p = 0.0001$ (Fig. 6J). Notably, there was also an increase in degenerative axons in the Nrf2 KO saline-injected mice in comparison to the wild-type saline controls, $p = 0.0263$ (Fig. 6J).

Similarly, there was a trend but no statistically significant difference in the VEP amplitude between the Nrf2 KO groups ($n = 14–16$ eyes for wildtype groups, $n = 8–12$ eyes for Nrf2 KO groups, $p = 0.2095$) (Fig. 6K). In contrast, the VEP amplitude of the Nrf2 KO mice was reduced in comparison to the wild-type counterparts ($p = 0.0093$, saline and $p < 0.0001$, microbead groups) (Fig. 6K). We also detected a decrease in the ERG b-wave amplitude, a measure of bipolar cell function, in the Nrf2 KO mice as compared to the wild-type mice at 2-wks post-IOP elevation ($p < 0.0001$ and $p = 0.002$ for saline and microbead injected, respectively; data not shown). And, similar to the

VEP results, there was no difference in the b-wave amplitudes between the Nrf2 KO saline-injected and microbead-injected mice ($p = 0.5359$; data not shown). Since the PhNR was reduced at 2-wks after microbead-injection in wild-type mice, we expected the amplitude to be decreased in the microbead-injected Nrf2 KO mice. However, while there was a trend, there was not a statistically significant difference in the PhNR amplitude between the Nrf2 KO saline-injected and the Nrf2 KO microbead-injected mice, $p = 0.1472$ (Fig. 6L). Similar to the VEP results, the Nrf2 KO saline-injected and microbead-injected mice had a significantly decreased amplitude in comparison to their respective wild-type controls ($p < 0.0001$, saline and $p = 0.0023$, microbead groups) (Fig. 6L).

### 4.6. Role of a compensatory mechanism in Nrf2 KO mice

One possible explanation for the lack of statistically significant deficit in the PhNR in the microbead-injected Nrf2 KO mice compared to the saline-injected Nrf2 KO mice is the presence of a partially effective compensatory mechanism. The ARE can be activated independent of NRF2 (for review see Raghunath et al., 2018). For example, NRF1 can act in place of NRF2 to increase gene expression of Nqo-1 and Ho-1, among others. Additionally, HIF-1α and HIF-1β comprise a complex that, when bound, can mediate transcription of a variety of genes downstream the Hypoxia Response Element, independent of the ARE [3,14,61]. Similar to how NRF2 senses and responds to increases in ROS, the HIF complex can sense changes in oxygen in its environment and can upregulate transcription of genes such as erythropoietin, Vegf, iNos and Slc2a1. We and others have previously demonstrated that erythropoietin is neuroprotective in glaucoma models [4,15,23,54,58,73].

The levels of HIF-1α protein were increased in both the Nrf2 KO groups in comparison to the wild-type controls ($n = 5$ retinas/group, $p = 0.0276$, saline and $p = 0.0021$ microbead groups) (Fig. 7A and B). There was no difference between the saline and microbead-injected Nrf2 KO groups ($p = 0.434$). The levels of NQO-1 and HO-1 were decreased in Nrf2 KO mice in comparison to wild-type controls (NQO-1: $p = 0.0048$ saline and $p = 0.0085$ microbead groups; HO-1: $p = 0.0013$ saline and $p = 0.0003$ microbead groups) (Fig. 7A, C). There was no significant difference in NQO-1 levels between the Nrf2 KO saline or microbead-injected groups, although levels seemed to trend up in the microbead injected mice ($p = 0.205$).

## 5. Discussion

Using an inducible model of glaucoma that provides tight temporal control on the same genetic background, we have confirmed that oxidative stress is an early event in glaucoma pathogenesis and have demonstrated a robust, but transient, endogenous antioxidant response that is mediated by the NRF2-KEAP1-ARE pathway. We show that this pathway is activated by phosphorylation of NRF2 by the PI3K/AKT pathway. Finally, we show that lack of Nrf2 results in the earlier onset of axon degeneration after induction of ocular hypertension.

We also discovered that the amplitude of the PhNR of the ERG is decreased early after IOP elevation, prior to axon degeneration or a decrease in the VEP. The early decrease in the PhNR amplitude might be explained by dendritic pruning and reduced RGC excitability, which was reported in a recent study [55]. Our data matches studies using different experimental glaucoma models, which have also shown a decrease in PhNR amplitudes in ocular hypertensive monkeys and rabbits [17,38].

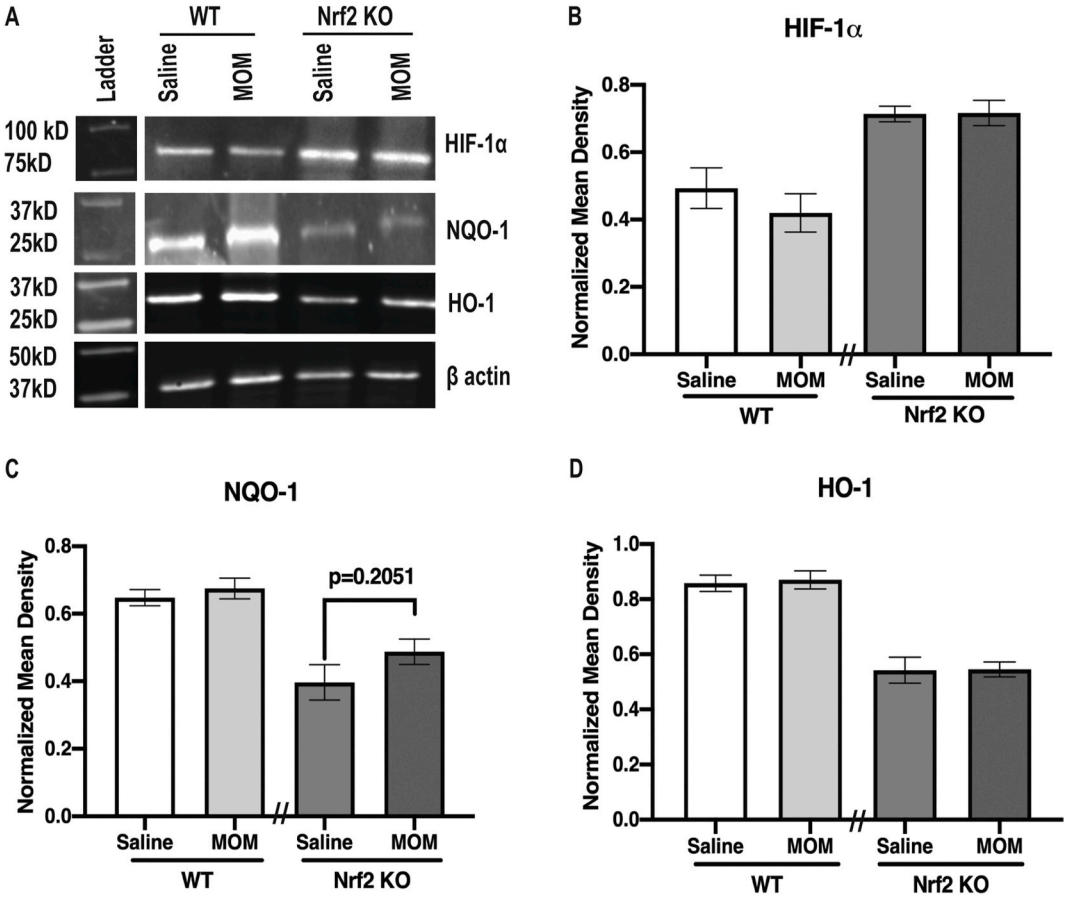


**Fig. 7.** Assessment of possible compensatory pathways. A) Representative western blots of HIF-1α, NQO-1, HO-1 and β-actin. B - D) Quantification of HIF-1α, NQO-1 and HO-1 western blots, respectively, after normalization to β-actin. HIF-1α was increased in both Nrf2 KO groups in comparison to wildtypes suggesting a compensatory response to the lack of NRF2. Both NQO-1 and HO-1 were decreased in both Nrf2 KO groups in comparison to wildtypes.

In addition, the diagnostic utility of the PhNR for patients who are glaucoma suspects has been demonstrated in multiple studies [10,38,41,50,51]. While the pattern ERG has also been suggested as a preclinical diagnostic for glaucoma and other RGC-related diseases, the PhNR has the advantage of not requiring refractive correction [51]. The PhNR could potentially be used as a pre-clinical, non-invasive biomarker for glaucoma diagnosis prior to onset of neuronal degeneration as ganglion cell function is disrupted in the MOM as early as 2-wks post-IOP elevation.

Levels of ROS were elevated in the retina prior to evidence of axon degeneration and were associated with a commensurate endogenous antioxidant response driven by the NRF2-KEAP1-ARE pathway. While a relationship between oxidative stress and experimental glaucoma is known [11,19,39,59], our findings confirm that ROS levels increase early after ocular hypertension using an inducible model, which provides tighter temporal control and allows for analysis on the same genetic background. Our results are consistent with those in the DBA/2J showing elevated *Gfap, Nos-2* and *Ho-1* levels in 3-month old mice, prior to any glaucomatous pathology, as compared to C57Bl/6 mice [26]. In a model of episcleral vein cauterization, there were increases in ROS, nitrite and lipid peroxidation levels as early as 1 day following injury [32]. In another model of ocular hypertension, where hyaluronic acid injections are used to elevate IOP, SOD and catalase levels were first increased at 3-wks, with pathology worsening up to 10-wks after injection [39]. Together, these studies suggest that quantification of retinal ROS might be a useful biomarker of early glaucoma. One *in vivo* assay of ROS being developed is QUEST-MRI (QUEnch-assiSTed), which quantifies production of endogenous ROS using hydrocyanine-800CW, which is an ROS-activated fluorescent probe [1,52]. Further, counteracting ROS might be an effective therapeutic strategy for early-stage glaucoma.

We detected no difference in total NRF2 at either the transcript or protein level in contrast to the decrease in NRF2 levels reported in an episcleral vein cauterization model (Arana et al., 2020). However, our detection of activation of NRF2 by PI3K and AKT is in agreement with previous findings showing that this pathway activates NRF2 in another study using the episcleral vein cauterization model of glaucoma in rats [28]. These pathways have also been linked to protection against oxidative stress in retinal pigment epithelial cells [18]. Further, this relationship has also been reported in models of chronic kidney disease and acute lung injury [5,47,57,64]. Exploring therapeutic options that increase levels or activation of NRF2 either directly or through an upstream activator could be an effective therapeutic strategy for glaucoma.

Our immunolabeling shows that the increased nitrotyrosine was present in the neurons of the ganglion cell layer, suggesting that the RGCs, not the glia, are the primary affected cells in this model of glaucoma. This is particularly true since peroxynitrite, the ROS responsible for the formation of nitrotyrosine residues, is highly reactive and thus unlikely to reach neighboring cells. Since the NRF2-KEAP1-ARE pathway is responsive to oxidative stress it is reasonable to hypothesize that activation of this pathway is occurring within the RGCs rather than neighboring glia. However, the fact that we detect activation of a signaling cascade and phosphorylation of NRF2 leaves open the possibility of cell to cell signaling. These two possibilities should be explored in future studies as it will direct therapeutic intervention to the appropriate cell type.

Previous studies have shown that adult Nrf2 KO mice have the same number of ganglion cells as a wild-type mouse prior to injury [22,37,65]. However, these studies did not involve an intraocular injection, nor did they assess visual function or optic nerve axons. Here, we show that Nrf2 KO mice given an intracameral injection of saline had increased levels of superoxide and greater axon degeneration and vision loss as compared to wild-type saline injected controls. This demonstrates the precarious environment in which the RGCs survive and their dependence on the NRF2-KEAP1-ARE pathway to remove any additional ROS insults. This result does match with our findings that an intraocular injection can be damaging to the optic nerve, particularly in the context of an ongoing insult to the optic nerve [42] studies showed that intravitreal injection of saline one day following injury via a model of indirect traumatic optic neuropathy causes greater axon degeneration, inflammation and visual function deficits at one month in comparison to mice that were injured but did not receive an intravitreal injection.

We examined the Nrf2 KO mice at 2-wks post-IOP elevation, a timepoint at which the only change detected in wildtype mice was a decrease in the amplitude of the PhNR. We detected a trend for a further decrease in both the PhNR and the VEP in the microbead-injected Nrf2 KO mice as compared to their saline controls, which were already reduced due to the injection effect. More striking, however, was the detection of fewer axons and more axon degeneration in the microbead-injected Nrf2 KO mice as compared to the saline-injected Nrf2 KO controls. This suggests an earlier onset of glaucomatous neurodegeneration when the Nrf2-KEAP1-ARE pathway is inactive.

We had expected a more robust deficit in the PhNR in the microbead injected Nrf2 KO mice. One rationale for the lack of a greater decrease is the presence of a partially effective compensatory, NRF2-independent, protective mechanism. We explored this by quantifying levels of antioxidant proteins whose expression levels can be increased through NRF2-independent pathways, i.e. HIF-1α, NQO-1 and HO-1 (for review see [77]). While there was less of an increase in Hif1α gene expression in the Nrf2 KO animals, there was an increase in protein levels. This suggests that there was less degradation of the HIF-1α protein in the Nrf2 KO mice, but the mechanism for this is unclear. Regardless, the increased level of HIF-1α could act on the Hypoxia Response Element and provide some protection to the retina and optic nerve. Importantly, HIF-1α was not further increased in the Nrf2 KO mice that had elevated IOP. Similarly, a previous study using Nrf2 KO mice in a model for wet age-related macular degeneration showed increased VEGF in comparison to wildtype controls suggesting increased activation of the HRE by HIF-1α [35,72]. In contrast, the levels of both NQO-1 and HO-1 were reduced in the Nrf2 KO mice suggesting that the associated NRF2 independent pathways were not upregulated. It is still feasible that another pathway, such as activation of AP1 on the ARE, [45,77,78] is also increased, resulting in minimal preservation of visual function. However, our data suggests that the NRF2-KEAP1-ARE pathway is the primary pathway used for endogenous antioxidant defenses in the retina in this model of glaucoma. This is in agreement with studies in other models of glaucoma or RGC death showing that Nrf2 KO mice do not have the antioxidant capacity to combat neuronal injury [27,66,69].

Importantly, the results from this study provide one explanation for the delay in glaucomatous neuronal degeneration in response to ocular hypertension. The activation of an antioxidant response by the retina decreases ROS levels and, thus, limits the amount of oxidative damage that occurs. However, the effect is transient and eventually the oxidative stress and resulting inflammation accumulates to a level that is damaging to the RGCs and pathology results. The results from this study also suggest that quantification of ROS and/or the PhNR could be useful biomarkers for early-stage glaucoma and that antioxidants could be an effective therapeutic, if given early.

## Funding

This work was supported by DoD W81XWH-15-1-0096 (TR), DoD W81XWH-17-2-0055 (TR), NEI R01 EY022349 (TR, DC), NEI R01 EY017427 (DC), NEI U24 EY029893 (TR), NEI U24 EY029903 (DC), Potocsnak Discovery Grant in Regenerative Medicine, Ayers Foundation Regenerative Visual Neuroscience Pilot Grant, Ret. Maj. General Stephen L. Jones, MD Fund, Stein Innovation Award (DC), Stanley Cohen Innovation Fund (DC), NEI P30EY008126 (VVRC), T32 EY021833 (VVRC) and Research Prevent Blindness, Inc Unrestricted Funds (VEI). The funding sources had no involvement in the study design, or collection, analysis, or interpretation of the data. The authors confirm that there are no known conflicts of interest associated with this

publication and there has been no significant financial support for this work that could have influenced its outcome.

## Declaration of competing interest

None.

## Acknowledgements

We thank Elisabeth Artis, Alexandra Bernardo-Colón, and Purnima Ghose for technical assistance.

## References

[1] B.A. Berkowitz, R.H. Podolsky, J. Lenning, N. Khetarpal, C. Tran, Wu, et al., Sodium iodate produces a strain-dependent retinal oxidative stress response measured in vivo using QUEST MRI, Invest. Ophthalmol. Vis. Sci. 58 (7) (2017) 3286–3293, https://doi.org/10.1167/iovs.17-21850.

[2] A. Bernardo-Colon, V. Vest, A. Clark, M.L. Cooper, D.J. Calkins, F.E. Harrison, et al., Antioxidants prevent inflammation and preserve the optic projection and visual function in experimental neurotrauma, Cell Death Dis. 9 (11) (2018), https://doi.org/10.1038/s41419-018-1061-4.

[3] C. Blancher, A.L. Harris, The molecular basis of the hypoxia response pathway: tumour hypoxia as a therapy target, Canc. Metastasis Rev. (1998), https://doi.org/10.1023/A:1006002419244.

[4] W.S. Bond, J. Hines-Beard, Yp L. Goldenmerry, M. Davis, A. Farooque, R. M. Sappington, et al., Virus-mediated EpoR76E therapy slows optic nerve axonopathy in experimental glaucoma, Mol. Ther. (2016), https://doi.org/10.1038/mt.2015.198.

[5] H.K. Bryan, A. Olayanju, C.E. Goldring, B.K. Park, The Nrf2 cell defence pathway: keap1-dependent and -independent mechanisms of regulation. Biochemical Pharmacology, 2013, https://doi.org/10.1016/j.bcp.2012.11.016.

[6] D.J. Calkins, Critical pathogenic events underlying progression of neurodegeneration in glaucoma, Prog. Retin. Eye Res. (2012), https://doi.org/10.1016/j.preteyeres.2012.07.001.

[7] D.J. Calkins, P.J. Horner, The cell and molecular biology of glaucoma: axonopathy and the brain, Invest. Ophthalmol. Vis. Sci. 53 (5) (2012) 2482–2484, https://doi.org/10.1167/iovs.12-9483i.

[8] M.J. Calkins, D.A. Johnson, J.A. Townsend, M.R. Vargas, J.A. Dowell, T. P. Williamson, et al., The Nrf2/ARE pathway as a potential therapeutic target in neurodegenerative disease, Antioxidants Redox Signal. (2009), https://doi.org/10.1089/ars.2008.2242.

[9] P. Chaudhary, F. Ahmed, P. Quebada, S.C. Sharma, Caspase inhibitors block the retinal ganglion cell death following optic nerve transection, Mol. Brain Res. 67 (1) (1999) 36–45, https://doi.org/10.1016/S0169-328X(99)00032-7.

[10] V. Chrysostomou, J.G. Crowston, The photopic negative response of the mouse electroretinogram: reduction by acute elevation of intraocular pressure, Invest. Ophthalmol. Vis. Sci. 54 (7) (2013) 4691–4697, https://doi.org/10.1167/iovs.13-12415.

[11] V. Chrysostomou, F. Rezania, I.A. Trounce, J.G. Crowston, Oxidative stress and mitochondrial dysfunction in glaucoma, Curr. Opin. Pharmacol. (2013), https://doi.org/10.1016/j.coph.2012.09.008.

[13] M. Culbreth, M. Aschner, GSK-3β, a double-edged sword in Nrf2 regulation: Implications for neurological dysfunction and disease, F1000Research (2018), https://doi.org/10.12688/f1000research.15239.1.

[14] V.L. Dengler, M.D. Galbraith, J.M. Espinosa, Transcriptional regulation by hypoxia inducible factors, Crit. Rev. Biochem. Mol. Biol. (2014), https://doi.org/10.3109/10409238.2013.838205.

[15] S. Ding, S. Leow, R. Munisvaradass, E. Koh, M. Bastion, K. Then, et al., Revisiting the role of erythropoietin for treatment of ocular disorders, Nat. Eye 30 (2016) 1293–1309, https://doi.org/10.1038/eye.2016.94.

[16] A.T. Dinkova-Kostova, R.V. Kostov, A.G. Kazantsev, The role of Nrf2 signaling in counteracting neurodegenerative diseases, FEBS J. 285 (19) (2018) 3576–3590, https://doi.org/10.1111/febs.14379.

[17] A.A. Elgohary, L.H.M. Elshazly, Photopic negative response in diagnosis of glaucoma: an experimental study in glaucomatous rabbit model, Int. J. Ophthalmol. 8 (3) (2015) 459–464, https://doi.org/10.3980/j.issn.2222-3959.2015.03.05.

[18] Z. Faghiri, N.G. Bazan, PI3K/Akt and mTOR/p70S6K pathways mediate neuroprotectin D1-induced retinal pigment epithelial cell survival during oxidative stress-induced apoptosis, Exp. Eye Res. 90 (6) (2010) 718–725, https://doi.org/10.1016/j.exer.2010.03.002.

[19] S.M. Ferreira, S. Fabián Lerner, R. Brunzini, C.G. Reides, P.A. Evelson, S.F. Llesuy, Time course changes of oxidative stress markers in a rat experimental glaucoma model, Invest. Ophthalmol. Vis. Sci. 51 (9) (2010) 4635–4640, https://doi.org/10.1167/iovs.09-5044.

[20] K. Fujita, K.M. Nishiguchi, Y. Shiga, T. Nakazawa, Spatially and temporally regulated NRF2 gene therapy using Mcp-1 promoter in retinal ganglion cell injury, Mol. Ther. Methods Clin. Dev. 5 (2017) 130–141, https://doi.org/10.1016/j.omtm.2017.04.003.

[21] I. Goldberg, Relationship between intraocular pressure and preservation of visual field in glaucoma, Surv. Ophthalmol. 48 (2 SUPPL. 1) (2003), https://doi.org/10.1016/S0039-6257(03)00006-7.

[22] N. Himori, K. Yamamoto, K. Maruyama, M. Ryu, K. Taguchi, M. Yamamoto, et al., Critical role of Nrf2 in oxidative stress-induced retinal ganglion cell death, J. Neurochem. 127 (5) (2013) 669–680, https://doi.org/10.1111/jnc.12325.

[23] J. Hines-Beard, W.S. Bond, J.R. Backstrom, T.S. Rex, Virus-mediated EpoR76E gene therapy preserves vision in a glaucoma model by modulating neuroinflammation and decreasing oxidative stress, J. Neuroinflammation (2016), https://doi.org/10.1186/s12974-016-0499-5.

[24] W. Huang, J.B. Fileta, T. Filippopoulos, A. Ray, A. Dobberfuhl, C.L. Grosskreutz, Hsp27 phosphorylation in experimental glaucoma, Invest. Ophthalmol. Vis. Sci. 48 (9) (2007) 4129–4135, https://doi.org/10.1167/iovs.06-0606.

[25] Y. Huang, W. Li, Z. Yuan Su, A.N.T. Kong, The complexity of the Nrf2 pathway: beyond the antioxidant response, JNB (J. Nutr. Biochem.) (2015), https://doi.org/10.1016/j.jnutbio.2015.08.001.

[26] D.M. Inman, W.S. Lambert, D.J. Calkins, P.J. Horner, α-Lipoic acid antioxidant treatment limits glaucoma-related retinal ganglion cell death and dysfunction, PloS One 8 (6) (2013), e65389, https://doi.org/10.1371/journal.pone.0065389.

[27] D.M. Inman, L. Coughlin, The role of Nrf2 transcription factor in ganglion cell survival in glaucoma, IOVS (Investig. Ophthalmol. Vis. Sci.) 55 (2424) (2014).

[28] A. Kanamori, M. Nakamura, Y. Nakanishi, A. Nagai, H. Mukuno, Y. Yamada, et al., Akt is activated via insulin/IGF-1 receptor in rat retina with episcleral vein cauterization, Brain Res. 1022 (1–2) (2004) 195–204, https://doi.org/10.1016/j.brainres.2004.06.077.

[29] H.E. Killer, A. Pircher, Normal Tension Glaucoma: Review of Current Understanding and Mechanisms of the Pathogenesis, /692/699/3161/3169/3170/692/699/3161 review-article. Eye (Basingstoke), 2018, https://doi.org/10.1038/s41433-018-0042-2.

[30] A. Kimura, X. Guo, T. Noro, C. Harada, K. Tanaka, K. Namekata, et al., Valproic acid prevents retinal degeneration in a murine model of normal tension glaucoma, Neurosci. Lett. 588 (2015) 108–113, https://doi.org/10.1016/j.neulet.2014.12.054.

[31] A. Kimura, K. Namekata, X. Guo, T. Noro, C. Harada, T. Harada, Targeting Oxidative Stress for Treatment of Glaucoma and Optic Neuritis, 2017, https://doi.org/10.1155/2017/2817252.

[32] M.L. Ko, P.H. Peng, M.C. Ma, R. Ritch, C.F. Chen, Dynamic changes in reactive oxygen species and antioxidant levels in retinas in experimental glaucoma, Free Radic. Biol. Med. 39 (3) (2005) 365–373, https://doi.org/10.1016/j.freeradbiomed.2005.03.025.

[33] Y. Koriyama, K. Chiba, M. Yamazaki, H. Suzuki, K. Ichiro Muramoto, S. Kato, Long-acting genipin derivative protects retinal ganglion cells from oxidative stress models in vitro and in vivo through the Nrf2/antioxidant response element signaling pathway, J. Neurochem. 115 (1) (2010) 79–91, https://doi.org/10.1111/j.1471-4159.2010.06903.x.

[34] Y. Koriyama, Y. Nakayama, S. Matsugo, S. Kato, Protective effect of lipoic acid against oxidative stress is mediated by Keap1/Nrf2-dependent heme oxygenase-1 induction in the RGC-5 cellline, Brain Res. 1499 (2013) 145–157, https://doi.org/10.1016/j.brainres.2012.12.041.

[35] S.E. Lacher, D.C. Levings, S. Freeman, M. Slattery, Identification of a functional antioxidant response element at the HIF1A locus, Redox Biol. 19 (2018) 401–411, https://doi.org/10.1016/j.redox.2018.08.014.

[36] L.A. Levin, C.L. Schlamp, R.L. Spieldoch, K.M. Geszvain, R.W. Nickells, Identification of the bcl-2 family of genes in the rat retina. https://iovs.arvojournals.org/article.aspx?articleid=2180650, 1997. (Accessed 20 August 2020).

[37] X.F. Liu, D.D. Zhou, T. Xie, J.L. Hao, T.H. Malik, Lu, et al., The Nrf2 signaling in retinal ganglion cells under oxidative stress in ocular neurodegenerative diseases, Int. J. Biol. Sci. (2018), https://doi.org/10.7150/ijbs.25996.

[38] S. Machida, Clinical applications of the photopic negative response to optic nerve and retinal diseases, J. Ophthalmol. (2012), https://doi.org/10.1155/2012/397178.

[39] M.C. Moreno, J. Campanelli, P. Sande, D.A. Sáenz, M.I. Keller Sarmiento, et al., Retinal oxidative stress induced by high intraocular pressure, Free Radic. Biol. Med. 37 (6) (2004) 803–812, https://doi.org/10.1016/j.freeradbiomed.2004.06.001.

[40] J.E. Morgan, Retina ganglion cell degeneration in glaucoma: an opportunity missed? A review, Clin. Exp. Ophthalmol. (2012), https://doi.org/10.1111/j.1442-9071.2012.02789.x.

[41] E.K.A. Morny, K. Patel, M. Votruba, A.M. Binns, T.H. Margrain, The relationship between the photopic negative response and retinal ganglion cell topography, Invest. Ophthalmol. Vis. Sci. 60 (6) (2019) 1879–1887, https://doi.org/10.1167/iovs.18-25272.

[42] S. Naguib, A. Bernardo-Colón, C. Cencer, N. Gandra, T.S. Rex, Galantamine protects against synaptic, axonal, and vision deficits in experimental neurotrauma, Neurobiol. Dis. 134 (2020), https://doi.org/10.1016/j.nbd.2019.104695.

[43] S. Naguib, A. Bernardo-Colón, T.S. Rex, Intravitreal injection worsens outcomes in a mouse model of indirect traumatic optic neuropathy from closed globe injury, Exp. Eye Res. (2020), https://doi.org/10.1016/j.exer.2020.108369.

[44] Y. Nakagami, Nrf2 Is an Attractive Therapeutic Target for Retinal Diseases, 2016, https://doi.org/10.1155/2016/7469326.

[45] T. Nguyen, H.C. Huang, C.B. Pickett, Transcriptional regulation of the antioxidant response element. Activation by Nrf2 and repression by MafK, J. Biol. Chem. 275 (20) (2000) 15466–15473, https://doi.org/10.1074/jbc.M000361200.

[46] T. Nguyen, P. Nioi, C.B. Pickett, The Nrf2-Antioxidant Response Element Signaling Pathway and its Activation by Oxidative Stress * ARE-Mediated Pathway, 2009, https://doi.org/10.1074/jbc.R900010200.

[47] S.K. Niture, R. Khatri, A.K. Jaiswal, Regulation of Nrf2 - an update, Free Radic. Biol. Med. (2014), https://doi.org/10.1016/j.freeradbiomed.2013.02.008.
[48] N.N. Osborne, S. Del Olmo-Aguado, Maintenance of retinal ganglion cell mitochondrial functions as a neuroprotective strategy in glaucoma, Curr. Opin. Pharmacol. (2013), https://doi.org/10.1016/j.coph.2012.09.002.
[49] M. Peng, L. Qiang, Y. Xu, C. Li, T. Li, J. Wang, Inhibition of JNK and activation of the AMPK-Nrf2 axis by corosolic acid suppress osteolysis and oxidative stress, Nitric Oxide Biol. Chem. (2019), https://doi.org/10.1016/j.niox.2018.11.002.
[50] V. Porciatti, Electrophysiological assessment of retinal ganglion cell function, Exp. Eye Res. (2014), https://doi.org/10.1016/j.exer.2015.05.008.
[51] D. Preiser, W.A. Lagrèze, M. Bach, C.M. Poloschek, Photopic negative response versus pattern electroretinogram in early glaucoma, Invest. Ophthalmol. Vis. Sci. 54 (2) (2013) 1182–1191, https://doi.org/10.1167/iovs.12-11201.
[52] M.C. Prunty, M.H. Aung, A.M. Hanif, R.S. Allen, M.A. Chrenek, Boatright, et al., In vivo imaging of retinal oxidative stress using a reactive oxygen species-activated fluorescent probe, Invest. Ophthalmol. Vis. Sci. 56 (10) (2015) 5862–5870, https://doi.org/10.1167/iovs.15-16810.
[53] W.S. Rasband, U.S. ImageJ, National Institutes of Health, Bethesda, Maryland, USA, http://imagej/nih.gov/ij/, 1997-2018.
[54] A.P. Resende, S.G. Rosolen, T. Nunes, B. Sao Braz, E. Delgado, Functional and structural effects of erythropoietin subconjunctival administration in glaucomatous animals, Biomed. Hub 3 (2018), 488970, https://doi.org/10.1159/000488970.
[55] M.L. Risner, S. Pasini, M.L. Cooper, W.S. Lambert, D.J. Calkins, Axogenic mechanism enhances retinal ganglion cell excitability during early progression in glaucoma, Proc. Natl. Acad. Sci. U. S. A 115 (10) (2018) E2393–E2402, https://doi.org/10.1073/pnas.1714888115.
[56] C. Saura, D. Roda, S. Roselló, M. Oliveira, T. Macarulla, Pérez-Fidalgo, et al., A first-in-human phase I study of the ATP-competitive AKT inhibitor Ipatasertib demonstrates Robust and safe targeting of AKT in patients with solid tumors, Canc. Discov. 7 (1) (2017) 102–113, https://doi.org/10.1158/2159-8290.CD-16-0512.
[57] E.A. Sivertsen, M.E. Hystad, K.B. Gutzkow, G. Døsen, E.B. Smeland, H.K. Blomhoff, et al., PI3K/Akt-dependent Epo-induced signalling and target genes in human early erythroid progenitor cells, Br. J. Haematol. 135 (1) (2006) 117–128, https://doi.org/10.1111/j.1365-2141.2006.06252.x.
[58] T.A. Sullivan, E.E. Geisert, J. Hines-Beard, T.S. Rex, Systemic adeno-associated virus-mediated gene therapy preserves retinal ganglion cells and visual function in DBA/2J glaucomatous mice, Hum. Gene Ther. (2011), https://doi.org/10.1089/hum.2011.052.
[59] G. Tezel, Oxidative stress in glaucomatous neurodegeneration: mechanisms and consequences, Prog. Retin. Eye Res. (2006), https://doi.org/10.1016/j.preteyeres.2006.07.003.
[60] C. Tonelli, I.I.C. Chio, D.A. Tuveson, Transcriptional regulation by Nrf2, Antioxidants Redox Signal. (2018), https://doi.org/10.1089/ars.2017.7342.
[61] R.K. Toth, N.A. Warfel, Strange bedfellows: nuclear factor, erythroid 2-Like 2 (Nrf2) and hypoxia-inducible factor 1 (HIF-1) in tumor hypoxia, Antioxidants (2017), https://doi.org/10.3390/antiox6020027.
[62] E.E. Vomhof-DeKrey, M.J. Picklo, The Nrf2-antioxidant response element pathway: a target for regulating energy metabolism, JNB (J. Nutr. Biochem.) (2012), https://doi.org/10.1016/j.jnutbio.2012.03.005.
[63] J. Vriend, R.J. Reiter, The Keap1-Nrf2-antioxidant response element pathway: a review of its regulation by melatonin and the proteasome, Mol. Cell. Endocrinol. (2015), https://doi.org/10.1016/j.mce.2014.12.013.
[64] L. Wang, Y. Chen, P. Sternberg, J. Cai, Essential roles of the PI3 kinase/Akt pathway in regulating Nrf2-dependent antioxidant functions in the RPE, Invest. Ophthalmol. Vis. Sci. (2008), https://doi.org/10.1167/iovs.07-1099.
[65] M. Wang, J. Li, Y. Zheng, The potential role of nuclear factor erythroid 2-related factor 2 (Nrf2) in glaucoma: a review, Med. Sci. Mon. Int. Med. J. Exp. Clin. Res. (2020), https://doi.org/10.12659/MSM.921514.
[66] X. Wang Zhi-lan Yuan, Activation of Nrf2/HO-1 Pathway Protects Retinal Ganglion Cells from a Rat Chronic Ocular Hypertension Model of Glaucoma, 2019, https://doi.org/10.1007/s10792-018-01071-8.
[67] R.N. Weinreb, T. Aung, F.A. Medeiros, The pathophysiology and treatment of glaucoma: a review, JAMA, J. Am. Med. Assoc. (2014), https://doi.org/10.1001/jama.2014.3192.
[68] M.P. Wymann, G. Bulgarelli-Leva, M.J. Zvelebil, L. Pirola, B. Vanhaesebroeck, M. D. Waterfield, et al., Wortmannin inactivates phosphoinositide 3-kinase by covalent modification of Lys-802, a residue involved in the phosphate transfer reaction, Mol. Cell Biol. 16 (4) (1996) 1722–1733, https://doi.org/10.1128/mcb.16.4.1722.
[69] Z. Xu, H. Cho, M.J. Hartsock, K.L. Mitchell, J. Gong, L. Wu, et al., Neuroprotective role of Nrf2 for retinal ganglion cells in ischemia-reperfusion, J. Neurochem. 133 (2) (2015) 233–241, https://doi.org/10.1111/jnc.13064.
[70] X. Yang, G. Hondur, G. Tezel, Antioxidant treatment limits neuroinflammation in experimental glaucoma, Invest. Ophthalmol. Vis. Sci. 57 (4) (2016), https://doi.org/10.1167/IOVS.16-19153.
[71] J. Zhao, S. Wang, W. Zhong, B. Yang, L. Sun, Y. Zheng, Oxidative stress in the trabecular meshwork (Review), Int. J. Mol. Med. (2016), https://doi.org/10.3892/ijmm.2016.2714.
[72] Z. Zhao, Y. Chen, J. Wang, P. Sternberg, M.L. Freeman, H.E. Grossniklaus, et al., Age-related retinopathy in NRF2-deficient mice, PloS One 6 (4) (2011), e19456, https://doi.org/10.1371/journal.pone.0019456.
[73] L. Zhong, J. Bradley, W. Schubert, E. Ahmed, A.P. Adamis, D.T. Shima, et al., Erythropoietin Promotes Survival of Retinal Ganglion Cells in DBA/2J Glaucoma Mice, vol. 48, 2007, pp. 1212–1218, https://doi.org/10.1167/iovs.06-0757.
[74] R.S. Sappington, B.J. Carlson, S.L. Crish, D.J. Calkins, The microbead occlusion model: a paradigm for induced ocular hypertension in rats and mice, Invest. Ophthalmol. Vis. Sci. 51 (1) (2010) 207–216, https://doi.org/10.1167/iovs.09-3947.
[75] N.J. Ward, K.W. Ho, W.S. Lambert, C. Weitlauf, D.J. Calkins, Absence of transient receptor potential vanilloid-1 accelerates stress-induced axonopathy in the optic projection, J. Neurosci. 34 (2014) 3161–3170, https://doi.org/10.1523/JNEUROSCI.4089-13.2014.
[76] N. Khan, I Ahman, T. Haqqi, Nrf2/ARE pathway attenuates oxidative and apoptotic response in human osteoarthritis chondrocytes by activating ERK1/2/ELK1-P70S6K-P90RSK signaling axis, Free Radic. Biol. Med. 116 (2018) 159–171, https://doi.org/10.1016/j.freeradbiomed.2018.01.013.
[77] A Raghunath, K Sundarraj, R Nagarajan, F Arfuso, J Bian, A Kumar, et al., Antioxidant response elements: Discovery, classes, regulation and potential applications, Redox Biol. 17 (2018) 297–314, https://doi.org/10.1016/j.redox.2018.05.002.
[78] F Soriano, P Baxter, L Murray, M Sporn, T.H. Gillingwater, G Hardingham, Transcriptional regulation of the AP-1 and Nrf2 target gene sulfiredoxin, Mol. Cells 27 (3) (2009) 279–282, https://doi.org/10.1007/s10059-009-0050-y.